The effect of primary crystallizing phases on mechanical properties of $Cu_{46}Zr_{47}Al_7$ bulk metallic glass composites

F. Jiang, Z.B. Zhang, L. He, and J. Sun[a]
State Key Laboratory for Mechanical Behavior of Materials, Xi'an Jiaotong University,
Xi'an 710049, People's Republic of China

H. Zhang and Z.F. Zhang
Shenyang National Laboratory for Materials Science, Institute of Metal Research, Chinese Academy
of Sciences, Shenyang 110016, People's Republic of China

$Cu_{46}Zr_{47}Al_7$ bulk metallic glass (BMG) and its composites in plate with different thicknesses up to 6 mm were prepared by copper mold casting. Primary crystallizing phases with different microstructures and volume fractions could be obtained under different cooling rates, forming some composites with different mechanical properties. Under compression tests, the 2-mm-thick monolithic BMG has a yield strength of 1894 MPa and a high fracture strength of up to 2250 MPa at plastic strain up to 6%, exhibiting apparent "work-hardening" behavior. The 4-mm-thick $Cu_{46}Zr_{47}Al_7$ BMG composite containing martensite phase yields at 1733 MPa and finally fails at 1964 MPa with a plastic strain of 3.7%.

I. INTRODUCTION

Recently, there has been considerable scientific and industrial interest in a variety of bulk metallic glass (BMG) composites as an effective way of further improving mechanical properties compared with monolithic BMGs.[1–9] In these composites, the second phase hinders single shear band to extend critically through the whole sample at the onset of plastic deformation and seeds the initiation of multiple shear bands. Therefore, plasticity is distributed more homogeneously in the shear band patterns, which results in local high strains to failure of the composites. The elements with high melting points, such as Ta, Nb, or Mo, are often added to ZrCu- and Ti-based BMGs by in situ precipitation of ductile micrometer-sized particles,[3,4] body-centered cubic-β (bcc-β) dendrites,[5,6] or nanostructure dendrites[7,8] upon cooling from the melting to improve the ductility of the composites. On one hand, the suitable composition design is important to ensure to high glass-forming ability (GFA) necessary for the formation of bulk amorphous matrix and to introduce an appropriate primary crystallizing phase. On the other hand, the size, geometry, and volume fraction of the primary crystallizing phase are also crucial for efficiently controlling of the shear band propagation and improving the ductility. Many efforts have been made to investigate the effect of alloy element addition on the microstructure and volume fraction of primary crystallizing phase.[7–9] However, there is little research[10,11] that deals with the microstructure and volume fraction of primary crystallizing phases under different cooling rates upon solidification.

Recently, it was reported that $Cu_{47.5}Zr_{47.5}Al_5$ BMG rod of 2 mm in diameter exhibited high compressive strength of up to 2265 MPa together with extensive "work hardening" and large plastic strain of 18%.[12] In addition, plasticity-improved Zr-Cu-Al BMG matrix composites were also prepared by in situ precipitation of CuZr martensite phase.[13] Compared with the former ZrCu- and Ti-based BMG composites,[1–9] Zr-Cu-Al (or Cu-Zr-Al) ternary alloys have a better combination of strength, ductility, and lower production cost. However, the Zr-Cu-Al BMGs and its composites with high strength and good ductility are seldom larger than 4 mm in diameter. The limited size makes it difficult to meet the requirement as structural materials.

In this article, a Zr-Cu-Al BMG and its composite plates with different thicknesses up to 6 mm were prepared by copper mold casting. The different thicknesses of the bulk samples lead to variable cooling rates upon solidification. The effect of the cooling rate on microstructures and volume fraction of primary crystallizing phase, as well as its mechanical properties, is systematically investigated.

II. EXPERIMENTAL PROCEDURES

In the present work, the tilt casting method in an arc furnace[14] was used to prepare BMGs and its composites. At the same time, the electromagnetic stirring function

was introduced to the equipment by adding a current loop under the water-cooled copper crucible.[15] The alloy ingots of nominal compositions $Cu_{46}Zr_{47}Al_7$ (at.%)[16] were prepared by arc melting mixtures of ultrasonically cleansed Zr (crystal bar, 99.9 at.%), Cu (99.99 at.%), and Al (99.99 at.%) pieces. The arc melting was performed in a Ti-gettered, high-purity argon atmosphere. Each ingot was re-melted at least four times, and electromagnetism stirring was used to ensure chemical homogeneity. The ingots were then cast into plates by copper mold casting. Plates with dimensions of $50 \times 20 \times h$ mm^3 ($h = 1.5, 2, 2.5, 3, 3.5, 4, 4.5, 5,$ and 6) were prepared and different thickness h lead to different cooling rates upon solidification for the casting BMG plates. The cooling rate was estimated from solution to the heat flow equation for a plate of liquid alloy cooled by heat conduction to a thick mold, which yields $R_C^{Plate} = 0.4K_tT_l/C_PL^2$,[17] with K_t as the thermal conductivity, C_P as the specific heat of the alloy, T_l as the melt temperature, and L as the plate's thickness. Taking $K_t \sim 0.1$ W/cm s^{-1} K^{-1} (typical of a molten alloys), $C_P \sim 4$ J/cm^3 K^{-1} (also typical of molten alloys), and $T_l \sim 1500$ K (for arc molten alloys). The oxygen content of the alloys was measured to be about 230 ppm. The transverse cross-section of the as-cast samples was analyzed with the x-ray diffraction (XRD) method with diffractometer (D/MAX-RB; Rigaku, Tokyo, Japan) using CuK$_\alpha$ radiation as a source. Standard transition electron microscope (TEM) observations were carried out using a TEM (JEM-200CX; JEOL, Tokyo, Japan) at 100 kV for a 2-mm-sample. A MeF3 ROTOSCOPE optical microscope (OM) was used for the microstructure observation. The volume fractions of crystalline phases in the alloys were evaluated by calculating the ratio of the heat released during annealing to the total crystallization enthalpy of the fully glassy alloy from differential scanning calorimeter (DSC) curves measured using DSC 2000 (Setaram Instrumentation, Caluire, France) with 800 °C rod (DSC) at a heating rate of 0.33K/s: $\%V_{crys} = (\Delta H_{max} - \Delta H)/\Delta H_{max}$,[18] where ΔH_{max} is the total enthalpy of transformation from the fully amorphous alloy to the completely crystallized alloy and ΔH from the tested samples. The samples for the compressive tests of $Cu_{46}Zr_{447}Al_7$ alloys were machined into different dimensions of $1.8 \times 1.8 \times 3.6$, $2.2 \times 2.2 \times 4.4$, $2.6 \times 2.6 \times 5.2$, $3.1 \times 3.1 \times 6.2$, $3.6 \times 3.6 \times 7.2$, $4.1 \times 4.1 \times 8.2$, $4.6 \times 4.6 \times 9.2$, and $5.6 \times 5.6 \times 11.2$ mm^3 specimens for the 2-, 2.5-, 3-, 3.5-, 4-, 4.5-, 5-, and 6-mm thick plates, respectively. Five specimens were used for each dimension. The compressive deformation was conducted on a computed-controlled, servo-hydraulic MTS 810 testing machine at a strain rate of 1×10^{-4} s^{-1} at room temperature. The yield point was determined at 0.2% plastic strain. The strain at the yield point corresponds to elastic strain and the strain at break point corresponds to total strain.

III. RESULTS AND DISCUSSION

Figure 1 shows the XRD patterns recorded from the cross-section of the as-cast alloys with different thicknesses. For the 1.5- and 2-mm samples, both of the patterns consist of only a series of broad diffraction maxima without any detectable sharp Bragg peaks. With the increase in the thickness, some detectable crystalline phases appear on the x-ray patterns. A few "spikes" were detected on the patterns of the 2.5-, 3-, and 3.5-mm samples, indicating that some crystals have precipitated. For the 4-mm sample, three small crystalline diffraction peaks superimposed on the broad amorphous diffraction peak were identified as CuZr phase. The crystalline phases in the 2.5-, 3-, and 3.5-mm samples should also be CuZr phase. For the 4.5-mm sample, other diffraction peaks identified as $Cu_{10}Zr_7$ were found except for CuZr phase. Zr_2Cu diffraction peaks were detected for the 5- and 6-mm samples in addition to CuZr and $Cu_{10}Zr_7$ phases. Similar diffraction peaks have also been found in the $Zr_{48.5}Cu_{46.5}Al_5$ alloy.[13] It should be noted that the solid solution of Al in CuZr induced the departure of crystalline diffraction peaks, and for the 4-mm-thick plate, there might be other crystallization phases that the XRD method could not distinguish.

It was pointed out by Chen and Spaepen[19] that isothermal calorimetric profiles could distinguish truly amorphous materials from "microcrystalline" materials that exhibited similarly broad diffraction halos. Truly amorphous materials exhibited exothermic peaks during isothermal scan, while microcrystalline materials released monotonically decaying heating flow signals. Hence, isothermal scanning was performed on the 2-mm-thick alloy at a constant temperature of 743 K. The apparent single exothermic peak characteristic of a nucleation
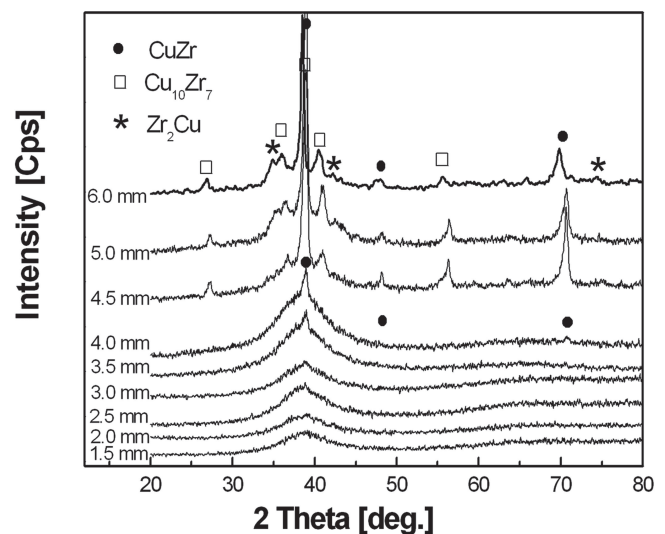

FIG. 1. XRD patterns of $Cu_{46}Zr_{47}Al_7$ alloys with different thicknesses.

and growth process confirms the as-cast glass structure of this alloy as concluded from its XRD pattern.[20] At the same time, the crystallization behavior of current Cu-Zr-Al system shows primary crystallization. It is reasonable to calculate the crystallized volume fraction from the enthalpy difference. The same method was also used by Bian et al.[6] to evaluate the volume fractions of crystalline phases in the Cu-Hf-Ti-Ag-Ta alloy. The DSC profiles of different thickness sample are shown in Fig. 2. It is obvious that the heat of crystallization decreases with increasing the thickness (1.5- and 2-mm samples are almost the same). The volume fractions of the crystalline phases calculated from DSC results for different thickness samples are listed in Table I. For the 1.5- and 2-mm samples, the volume fractions of crystalline phases are close to zero. The volume fractions of crystalline phases in the 2.5-, 3-, 3.5-, 4-, 4.5-, 5-, and 6-mm samples are equal to 4.2%, 8.3%, 23.9%, 33.0%, 86.8%, 92.1%, and 100%, respectively. It is surprising that the 4-mm-thick sample actually contains 33.0% crystalline phases in volume, and its XRD pattern shows there is only a small amount of crystalline phases. There may be many microcrystallines in this sample, which exhibits similarly broad diffraction halos as fully amorphous alloy. The estimated cooling rates of different thick plates are also listed in Table I. The critical cooling rate of this $Cu_{46}Zr_{47}Al_7$ alloy to form fully amorphous is about 370 K/s (estimated from the 2-mm plate). Crystallizing phase CuZr precipitates at a cooling rate less than 370 K/s. When the cooling rate is less than 90 K/s (estimated from the 4-mm plate), a large number of other crystalline phases such as $Cu_{10}Zr_7$ precipitates appears. It is also found that the volume fraction of the crystalline phase increases dramatically from 33.0%–86.8% as the cooling rate
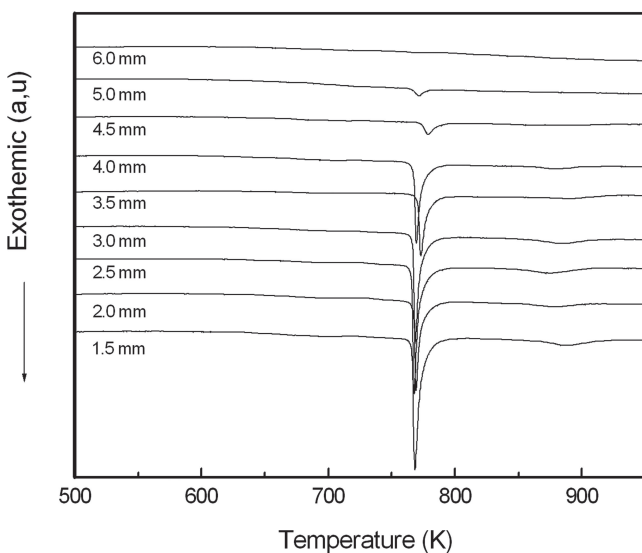
decreases from 90–70 K/s (plate thickness changed from 4 to 4.5 mm).

The OM observation was undertaken to examine the microstructures in the center of the cross-sectional areas of all the alloys with different thickness. It reveals there is not any visible crystallization phase in the 2-mm sample [see Fig. 3(a)]. The TEM selected-area diffraction patterns for the 2-mm-thick sample is presented in the inset of Fig. 3(a). According to the results of XRD, DSC traces, and OM and TEM observations, it can be concluded that the 2-mm sample has a fully glassy structure. It was reported that the ratio of the maximum dimension of casting plate thickness L_{plate} to the rod diameter L_{rod} follows the relation $L_{plate}:L_{rod}$ = 1:1.7.[21] For the present plate specimens, the 2-mm-thick BMG plate is equal to 3.4-mm rods in diameter processed by the same copper mold method, and the GFA of this $Cu_{46}Zr_{447}Al_7$ is about 3 mm in diameter, which is in agreement with the report in Ref. 16. The 4-mm-thick plate is equal to 6.8-mm rods in diameter. With the decreasing cooling rate upon solidification, CuZr primary crystallizing phase began to appear, and its size, amount, and microstructure varied with the cooling rate. Figures 3(b)–3(h) illustrate the evolution processes of submicrostructures in grains during the decrease in the cooling rate. Figures 3(b)–3(d) show that in the 2.5-, 3-, and 3.5-mm samples, there are many dispersed small dendrites within the round grains that emerged and grew bigger with the decrease in cooling rate. After this, a regular radial distribution of dendrites [see Fig. 3(e)] can be found in those bigger grains, which locate mainly between the edge and center of the 4-mm sample and is not observed in the 2.5-, 3-, and 3.5-mm samples. Blocky grains with different sizes within a bigger grain can be found mainly in the center part of the 4-mm sample, where the cooling rate is lower than that of sample edge. The blocky grains display an uneven surface and contain plates with different lengths inside, as shown in Fig. 3(f). The plates are self-arranged and align in different subcrystalline regions. The surface morphology of the grains reveals that a martensite phase might form during the rapid cooling of the alloy melts, as identified by CuZr phase in the XRD pattern. Similarly, in the $Zr_{48.5}Cu_{46.5}Al_5$ alloy,[13] these grains have been confirmed as CuZr martensite phases. For the 2.5-, 3-, 3.5-, and 4-mm plates, all of the crystallization phases are CuZr. There is an obvious microstructure transition of crystallizing CuZr with the decrease of cooling rate: disperse small dendrites—regular radial dendrites—martensite phase structure. Similarly, there also exists an obvious microstructure transition from the center region to the edge from the difference in the cooling rate. Figure 3(i) shows that the whole cross-section of the 4-mm sample and grains with various submicrostructures could be found in the different regions of the cross-section.

FIG. 2. DSC traces of $Cu_{46}Zr_{447}Al_7$ alloys with different thicknesses at a heating rate of 0.33 K/s.

TABLE I. Summary of processing parameters, resulting structures, and mechanical properties for $Cu_{46}Zr_{47}Al_7$ alloy.

Sample (mm)	R_C^{Plate} (K/s) [17]	V_{crys} (%)	ϵ_p (%)	σ_s (MPa)	$\sigma_{c,f}$ (MPa)	Structure
1.5	670	0				Glass
2	370	0	6	1894	2250	Glass
2.5	240	4.2	2.97	1890	2056	Glass + CuZr (dendrites)
3	170	8.3	2.11	1817	1933	Glass + CuZr (dendrites)
3.5	120	23.8	0.6	1750	1848	Glass + CuZr (dendrites)
4	90	33.1	3.7	1733	1964	Glass + CuZr (martensite + dendrites)
4.5	70	86.8	2	900	1440	Glass + CuZr + $Cu_{10}Zr_7$
5	60	92.1	2.55	546	1308	Glass + CuZr + $Cu_{10}Zr_7$ + Zr_2Cu
6	40	100	3	384	1224	CuZr + $Cu_{10}Zr_7$ + Zr_2Cu

With a further decrease in the cooling rate, apart from CuZr and $Cu_{10}Zr_7$ phases precipitated in the 4.5-mm sample, the amount of the martensite phase begins to reduce [comparing the center parts of Figs. 3(f) and 3(g)]. In the 5-mm sample, CuZr $Cu_{10}Zr_7$ and Zr_2Cu phases were all detected, and as indicated in Fig. 3(h), there are many small grains instead of martensite phase because the reduced cooling rate induced more crystallization and there is not enough space to grow bigger. It could be found that martensite phase transformation only occurs at a certain cooling rate. When the cooling rate is 120 K/s (estimated from the 3.5-mm plate), there is no martensite phase. Martensite phase transformation occurs at a cooling rate of about 90 K/s.

Figure 4 presents the compressive engineering stress-strain curves for the alloys investigated. The variation of yield strength, fracture strength, and plastic strain to fracture of samples with different volume fractions of crystalline phases are listed Table I. It can be seen that the 2-mm specimen yields at a stress of about 1894 MPa and fails at a stress of up to 2250 MPa. It exhibits apparent "work hardening" with significant plastic strain up to 6%. The true stress-strain curve of $Cu_{46}Zr_{47}Al_7$ is presented in the inset of Fig. 4. It is very clear that there is an increase of the flow stress after yielding. Recently, a $Cu_{47.5}Zr_{47.5}Al_5$ alloy, which 5% (at.%) Al was added into $Cu_{50}Zr_{50}$, exhibits a high strength of up to 2265 MPa together with extensive work hardening and a large plastic strain of 18%.[12] The present $Cu_{46}Zr_{47}Al_7$ alloy has a similar composition as the $Zr_{47.5}Cu_{47.5}Al_5$ alloy. The nature of the work-hardening capability and ductility of the current metallic glass should be same as that of $Zr_{47.5}Cu_{47.5}Al_5$ alloy and is attributed to a unique structure correlated with atomic-scale inhomogeneity, leading to an inherent capability of extensive shear band formation, interactions, and multiplication of shear bands.[12] At the same time, the 1- to 2-nm scale medium-range ordering might responsible for the high strength, significant work hardening, and large plasticity of the samples, which have been revealed by HRTEM investigations in fully metallic glassy $Cu_{50}Zr_{50}$ rods of 1.5 mm diameter.[22]

For the 2.5-, 3-, and 3.5-mm samples, all of the yield and fracture strengths decreased with the increase in thickness. Their plastic strains to fracture are 3.0%, 2.1%, and 0.6%, respectively. The 2.5-, 3-, and 3.5-mm samples contain 4.2%, 8.3%, and 23.9% crystalline phases, respectively, and there are mainly round grains with disperse small dendrites as submicrostructure precipitated in them. Leonhard et al.[23] have suggested that quenched-in crystalline is the weak spot in a Zr-based alloy where crack initiation preferentially occurs and propagates easily. The precipitation of crystallites leads to the softening of the remaining matrix. The mixed structure of crystallites embedded on the softening amorphous matrix initiate cracks more easily or can speed up the propagation of cracks, furthermore leading to embrittlement of the alloys. At the same time, the precipitation of crystalline phases also decreases their yield strengths. In the present alloys, these disperse small dendrites have deteriorated the ductility and yield strength. In particular, 23.9% crystalline phases dispersed in small dendrites in the 3.5-mm sample seriously reduces the ductility to 0.6%.

For the 4-mm and thicker samples, they all display obvious strain hardening and obvious plastic deformation before failure. The 4-mm sample shows a yield strength of 1733 MPa, a fracture strength of 1964 MPa, and a plastic strain of 3.7% to fracture. For the 4.5-, 5-, and 6-mm samples, their plastic strains to fracture are 2.0%, 2.6%, and 3.0%, respectively. And their yield strengths are 900, 546, and 384 MPa, respectively, which are much lower than that of the 4-mm sample. The surface deformation feature of the 3.5-, 4-, and 4.5-mm samples are shown in Fig. 5. There are fewer visible shear bands on the side surface of the 3.5-mm sample [see Fig. 5(a)] and its plasticity strain to fracture is only 0.6%. Figure 5(b) shows that dense shear bands were activated on the side surface of the 4-mm sample. Primary shear bands are inclined at an angle of about 45 degrees to the loading direction. The secondary and tertiary shear bands on the deformation surface interact with each other, forming numerous branches. The presence of dense shear bands indicates that the composites have good ductility and can
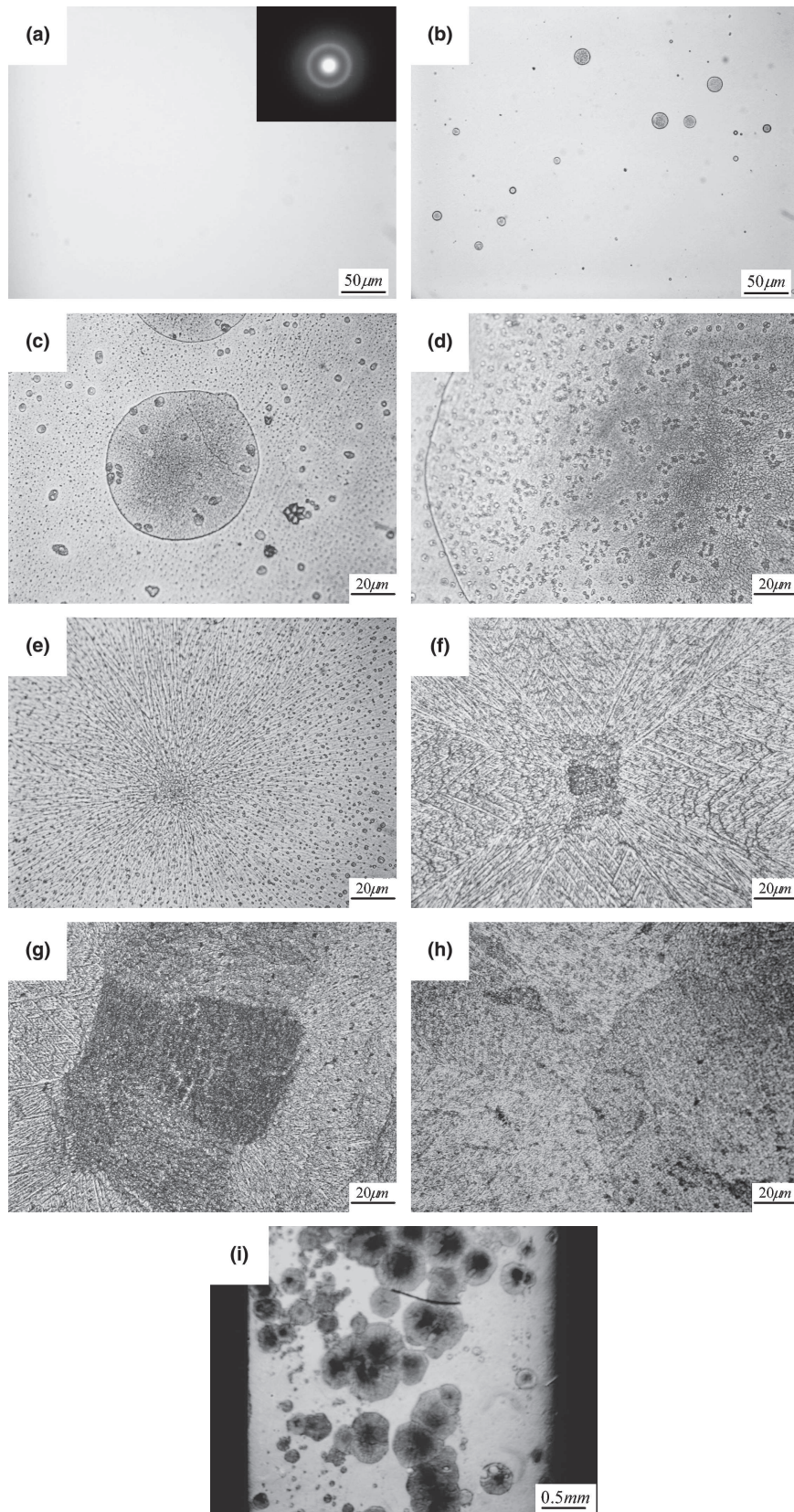
J. Mater. Res., Vol. 21, No. 10, Oct 2006

2641

FIG. 3. (a) Optical images of microstructures in the center of the cross-sectional areas of $Cu_{46}Zr_{447}Al_7$ alloys for the 2-mm sample; the inset shows its TEM selected-area diffraction patterns: (b–d) 2.5-, 3-, and 3.5-mm samples, (e–g) 4-mm sample, (h) 5-mm sample. (i) Whole cross section of the 4-mm sample.
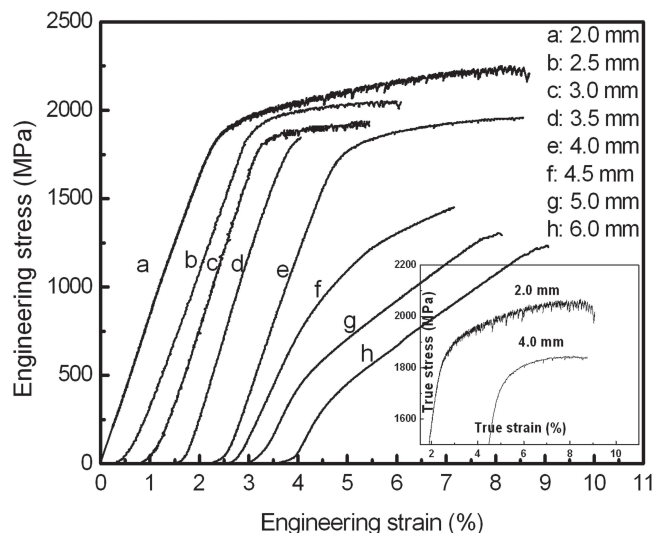
FIG. 4. Compressive stress-strain curves of $Cu_{46}Zr_{47}Al_7$ alloys with different thicknesses.

be deformed by the formation and propagation of multiple shear bands. It is believed that the micrometer-sized CuZr martensite phase might experience strain hardening and act as an obstacle to the local shear deformation, thus retarding the shear fracture of the alloy.[13] Compared with the grains with disperse small dendrites or regular radial dendrites, the grains with CuZr martensite phase structure more efficiently control the shear band propagation. The ductility of the 4-mm sample is still lower than that of the 2-mm-thick monolithic BMG because there are grains with various submicrostructures in the different regions of the 4-mm sample in which disperse small

dendrites reduce the ductility, and martensite phase structures improve the ductility. Figure 5(c) shows that the number of shear bands in the 4.5-mm sample is in between that of the 3.5- and 4-mm samples and its plasticity strain to fracture is about 2%. Secondary cracks could also be found on the side surface from the precipitation of brittle $Cu_{10}Zr_7$ phase. For the 4.5-, 5-, and 6-mm samples, the precipitation of brittle $Cu_{10}Zr_7$ and Zr_2Cu phases deteriorate their ductility. At the same time, the yield strengths are reduced severely, owing to the existence of large number of brittle $Cu_{10}Zr_7$ and Zr_2Cu phases.

The processing parameters, resulting structures, and mechanical properties for $Cu_{46}Zr_{47}Al_7$ alloy are summarized in Table I. It can be found that the 2-mm-thick monolithic BMG has the highest yield strength and best ductility among the Zr-Cu-Al alloys. The yield strength decreases with increasing the volume fraction of crystalline phases from the decrease of cooling rate. For example, the yield strength of the 4- and 4.5-mm samples decreases dramatically from 1733–900 MPa, when the volume fraction of crystalline phases increases from 33.0% to 86.8%. For the 5- and 6-mm sample containing 92% and 100% crystalline phases, their yield strengths are even decreased to 546 and 384 MPa, which are comparable with those of common carbon steels. Although sometimes the primary crystallizing phase is beneficial to the ductility, appropriate volume fraction of crystalline phases should be concerned with the aim of obtaining the optimum composite with good ductility and high yield strength. For the in situ composites, its ductility is always reduced because of the precipitation of
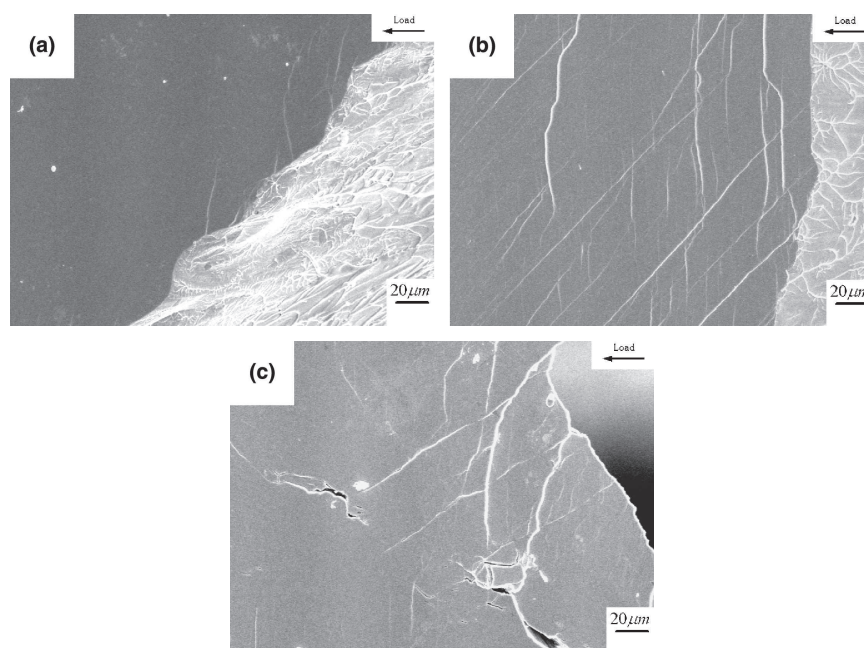

FIG. 5. The shear bands of fracture specimens side surfaces: (a) 3.5 mm, (b) 4 mm, and (c) 4.5 mm.

crystalline phases. However, the grains with CuZr martensite phase structure more efficiently control the shear band propagation than the grains with disperse small dendrites or regular radial dendrites, and the 4-mm-thick $Cu_{46}Zr_{47}Al_7$ BMG composite containing martensite phase displays a better ductility than 2.5-, 3-, and 3.5-mm samples.

Recently, Ma and Chang[24] had elucidated the formation of metallic glasses and glass-matrix composites in ternary eutectic systems with the competitive growth principle with the premise that glass formation competes with the growth of all the possible crystalline structures. The formation of two types of glass-matrix composites, i.e., single-phase dendrites plus a glass, and single-phase dendrites plus a two-phase eutectic plus a glass, has been predicted as a result of the incomplete suppression of growth of the primary and/or secondary competing structures. Wang et al.[25] pointed out the three best glass-forming regions in three adjacent eutectics in the ternary Zr-Cu-Al (or Cu-Zr-Al) system, and there is a strong dependency of GFA on composition; even a 1 at.% difference would significantly change the GFA of the sample. They also reported the existence of three glass matrix composite-forming regions (i.e., τ_5 + glass, ZrCu + glass, and $Cu_{10}Zr_7$ + glass). For the present work, a Zr-Cu-Al ternary alloy composite composed of glass plus a single primary crystallizing phase was obtained. It can be found that the predication of Ma and Chang[24] is consistent with the experimental works of Wang et al.[25] and this article: that composite with glass and single-phase crystalline can be obtained in certain compositions in a ternary alloy system. In the present alloy, primary-crystallizing phases with different microstructures and volume fractions can be obtained under different cooling rates. Especially, CuZr martensite phase as a primary crystallizing phase can be formed under a certain cooling rate, which improves the plasticity of the composite. Similar martensite phases as primary crystallizing phases can also be found in the plasticity-improved $Zr_{48.5}Cu_{46.5}Al_5$ alloy.[13] It is reasonable to consider that martensite phase as a primary crystallizing phase might be formed in other Zr-Cu-Al alloys under certain cooling rates, and BMGs composites composed of optimum crystalline and glass in the Zr-Cu-Al ternary system can be developed through optimum composition design and cooling rate control.

IV. CONCLUSION

The effect of microstructures and volume fraction of primary crystallizing phases on mechanical properties of $Cu_{46}Zr_{47}Al_7$ BMG composites under different cooling rates were investigated. Different crystallizing phases with variable volume fraction and microstructures were

found in the $Cu_{46}Zr_{47}Al_7$ BMG composites with different thickness. Under compression test, the 2-mm-thick monolithic BMG sample has yield strength of 1894 MPa, a high fracture strength of up to 2250 MPa, and exhibits apparent work hardening with a significant plastic strain up to 6%. The 4-mm-thick $Cu_{46}Zr_{47}Al_7$ BMG composite containing a martensite phase yields at 1733 MPa, fails at 1964 MPa, and exhibits apparent work hardening with a good plastic strain up to 3.7%.

ACKNOWLEDGMENTS

REFERENCES

1. H. Kato, T. Hirano, A. Matsuo, Y. Kawamura, and A. Inoue: High strength and good ductility of $Zr_{55}Al_{10}Ni_5Cu_{30}$ bulk glass containing ZRC particles. *Scripta Mater.* **43,** 503 (2000).

2. H. Choi-Yim, R. Busch, U. Koster, and W.L. Johnson: Synthesis and characterization of particulate reinforced $Zr_{57}Nb_5Al_{10}Cu_{15.4}Ni_{12.6}$ bulk metallic glass composites. *Acta Mater.* **47,** 2455 (1999).

3. C. Fan, R.T. Ott, and T.C. Hufnagel: Metallic glass matrix composite with precipitated ductile reinforcement. *Appl. Phys. Lett.* **81,** 1020 (2002).

4. J.C. Lee, Y.C. Kim, J.P. Ahn, H.S. Kim, S.H. Lee, and B.J. Lee: Deformation-induced nanocrystallization and its influence on work hardening in a bulk amorphous matrix composite. *Acta Mater.* **52,** 1525 (2004).

5. C.C. Hays, C.P. Kim, and W.L. Johnson: Microstructure controlled shear band pattern formation and enhanced plasticity of bulk metallic glasses containing in situ formed ductile phase dendrite dispersions. *Phys. Rev. Lett.* **84,** 2901 (2000).

6. Z. Bian, H. Kato, C.L. Qin, W. Zhang, and A. Inoue: Cu-Hf-Ti-Ag-Ta bulk metallic glass composites and their properties. *Acta Mater.* **53,** 2037 (2005).

7. G. He, J. Eckert, W. Loser, and L. Schultz: Novel Ti-base nanostructure-dendrite composite with enhanced plasticity. *Nat. Mater.* **2,** 33 (2003).

8. G. He, W. Loser, and J. Eckert: In situ formed Ti-Cu-Ni-Sn-Ta nanostructure-dendrite composite with large plasticity. *Acta Mater.* **51,** 5223 (2003).

9. T.C. Hufnagel, C. Fan, R.T. Ott, J. Li, and S. Brennan: Controlling shear band behavior in metallic glasses through microstructural design. *Intermetallics* **10,** 1163 (2002).

10. Z. Bian, G.L. Chen, G. He, and X.D. Hui: Microstructure and ductile-brittle transition of as-cast Zr-based bulk glass alloys under compressive testing. *Mater. Sci. Eng., A* **316,** 135 (2001).

11. U. Kuhn, J. Eckert, N. Mattern, and L. Schultz: Microstructure and mechanical properties of slowly cooled Zr-Nb-Cu-Ni-Al composites with ductile bcc phase. *Mater. Sci. Eng., A* **375,** 322 (2004).

12. J. Das, M.B. Tang, K.B. Kim, R. Theissmann, F. Baier,

W.H. Wang, and J. Eckert: "Work-hardenable" ductile metallic glass. *Phys. Rev. Lett.* **94,** 205501 (2005).

13. Y.F. Sun, B.C. Wei, Y.R. Wang, W.H. Li, T.L. Cheung, and C.H. Shek: Plasticity-improved Zr-Cu-Al bulk metallic glass matrix composites containing martensite phase. *Appl. Phys. Lett.* **87,** 051905 (2005).

14. Y. Yokoyama, K. Fukaura, and A. Inoue: Cast structure and mechanical properties of Zr-Cu-Ni-Al bulk glassy alloys. *Intermetallics* **10,** 1113 (2002).

15. F. Jiang, Z.J. Wang, Z.B. Zhang, and J. Sun: Formation of Zr-based bulk metallic glasses from low purity materials by scandium addition. *Scripta Mater.* **53,** 487 (2005).

16. D.H. Xu, G. Duan, and W.L. Johnson: Unusual glass-forming ability of bulk amorphous alloys based on ordinary metal copper. *Phys. Rev. Lett.* **92,** 245504 (2004).

17. B. Lohwongwatana, J. Schroers, and W.L. Johnson: Strain rate induced crystallization in bulk metallic glass-forming liquid. *Phys. Rev. Lett.* **96,** 075503 (2006).

18. T. Gloriant and A.L. Greer: Al-based nanocrystalline composites by rapid solidification of Al-Ni-Sm alloys. *Nanostruct. Mater.* **10,** 389 (1998).

19. L.C. Chen and F. Spaepen: Calorimetric evidence for the micro-quasicrystalline structure of "amorphous" Al-transition metal alloys. *Nature* **336,** 6197 (1988).

20. F. Jiang, Z.B. Zhang, J. Zhang, L. He, and J. Sun: Bending ductility and shear band spacing of copper-based metallic glass plate. *Acta Metall. Sinica* **41,** 1031 (2005).

21. I.I. Konovalov, V.A. Komissarov, A.A. Maslov, and V.K. Orlov: Bulk amorphous plate production by a casting process. *J. Non-Cryst. Solids* **207,** 536 (1996).

22. Z.W. Zhu, H.F. Zhang, W.S. Sun, B.Z. Ding, and Z.Q. Hu: Processing of bulk metallic glasses with high strength and large compressive plasticity in $Cu_{50}Zr_{50}$. *Scripta Mater.* **54,** 1145 (2006).

23. A. Leonhard, L.Q. Xing, M. Heilmaier, A. Gebert, J. Eckert, J. Schultz, and L. Schultz: Effect of crystalline precipitations on the mechanical behavior of bulk glass forming Zr-based alloys. *Nanostruct. Mater.* **10,** 805 (1998).

24. D. Ma and Y.A. Chang: Competitive formation of ternary metallic glasses. *Acta Mater.* **54,** 1927 (2006).

25. D. Wang, H. Tan, and Y. Li: Multiple maxima of GFA in three adjacent eutectics in Zr-Cu-Al alloy system: A metallographic way to pinpoint the best glass forming alloys. *Acta Mater.* **53,** 2969 (2005).